Available online at www.sciencedirect.com
SCIENCE DIRECT®
Catalysis Today 96 (2004) 71–78
CATALYSIS TODAY
www.elsevier.com/locate/cattod

NO_x storage on BaO: theory and experiment

Peter Broqvist [a,*], Henrik Grönbeck [a], Erik Fridell [a], Itai Panas [b]

[a] *Department of Applied Physics and Competence Centre for Catalysis, Chalmers University of Technology, Sweden*
[b] *Department of Environmental Inorganic Chemistry, Chalmers University of Technology, Göteborg SE 412-96, Sweden*

Available online 25 June 2004

Abstract

We review our understanding of the NO_2 interaction with BaO. The presented picture has evolved from calculations using the density functional theory, reactor measurements and vibrational spectroscopy of surface species during NO_2 storage on a BaO/Al_2O_3 catalyst and BaO powder. The DFT calculations predict nitrite formation on the BaO(1 0 0) surface upon NO_2 adsorption. A particular stable adsorption configuration is a nitrate–nitrite pair geometry, with the nitrate bonded to a barium cation and the nitrite involving a surface oxygen anion. This configuration is supported by vibrational spectroscopy. Only nitrite formation is observed for NO_2 exposure to BaO powder at low temperatures, whereas signatures at ~250 °C reveal the formation of surface nitrates. Continuous NO_2 adsorption at this temperature results in surface $Ba(NO_3)_2$, as well as bulk $Ba(NO_3)_2$, formation.
© 2004 Elsevier B.V. All rights reserved.

Keywords: NO_x storage; BaO; Slab; Cluster; Surface properties; DFT; CPMD; DRIFT; Vibrational properties

1. Introduction

The increasing emissions of green-house gases have stimulated new strategies for fossil fuel combustion in transport applications. The objective is to decrease the amount of carbon dioxide emissions by increasing the combustion efficiency, using lean-burn or diesel engines. However, gasoline engines operating at high air-to-fuel ratios prevents the use of the conventional three-way catalyst for NO_x reduction, as the three-way activity (simultaneous oxidation of carbon monoxide and hydrocarbons, and reductions of NO_x) is restricted to stoichiometric combustion. In fact, it is this limitation of the three-way catalyst that presently hinders the use of more fuel efficient gasoline engines.

A possible solution to the problem with NO_x reduction during lean combustion is the, so called, NO_x storage and reduction (NSR) concept [1,2]. The principle of this methodology is schematically shown in Fig. 1. The materials in the catalyst are the same as for the three-way catalyst with the addition of a NO_x trapping agent. The NSR concept is built upon a periodically lean/rich engine operation. During long lean periods, NO_x is stored on the trapping agent. This NO_x is released during short rich pulses, and subsequently reduced by hydrocarbons, CO, and hydrogen over noble metal sites to form CO_2, N_2, and water.

The NO_x trapping materials can be found among the alkali and alkaline earth metal oxides, where BaO has been most extensively studied experimentally. These oxides are, however, also efficient for CO_x and SO_x storage. Thus in the presence of CO_2 there will be a competition between NO_x and CO_x adsorption. For BaO, this is not a major issue since surface carbonates have been shown to be less stable than surface NO_x species at ambient temperatures [3]. A more severe problem is emissions of SO_x, which reduces the efficiency of both the storage material and the catalytically active material [4]. Presently, the only plausible solution to this problem is the use of fuel with low sulfur content. In addition to CO_x and SO_x resistance, NO_x trapping materials must meet temperature and ageing demands. In order to improve the storage materials with respect to selectivity and temperature resistance, fundamental understanding of the governing processes is necessary. In previous publications [5,6], we have focused on the storage scenario, and studied different aspects of the NO_x interaction. This work will be reviewed below. Other theoretical reports in the literature include NO_2 adsorption on MgO [7–9] as well as for the complete series of alkaline earth metal oxides [10,11]. Despite the documented reactivity of BaO terrace sites,

* Corresponding author. Tel.: +46 31 772 4541; fax: +46 31 772 3134.
E-mail address: p.broqvist@fy.chalmers.se (P. Broqvist).

0920-5861/$ – see front matter © 2004 Elsevier B.V. All rights reserved.
doi:10.1016/j.cattod.2004.05.009

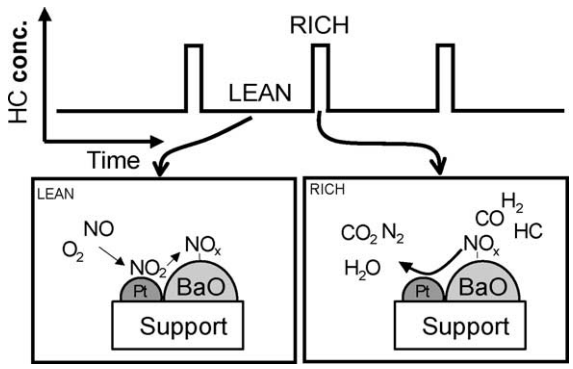

Fig. 1. Schematic representation of the NSR principle. The engine is operated periodically. During lean operation of the engine, NO_x is stored on the trapping material and during short fuel rich pulses, the stored NO_x is released and subsequently reduced over platinum sites on the catalyst.

the importance of steps and corners of BaO for enhanced NO_x adsorption have been discussed, and an increased reactivity for such sites have been reported in the literature [12].

2. Theoretical and experimental approaches

2.1. Theoretical approach

The density functional theory (DFT) [13,14] has grown into the standard theoretical frame-work for large scale first principles calculations. In the present studies, we have used DFT in the implementation with plane waves and pseudopotentials [15–19]. Two different strategies for describing the metal-oxide has been explored. The periodic supercell method and the finite cluster method. Both strategies have been used previously in the literature for description of adsorbate/metal-oxide interactions [20]. Generally it is unclear which method that most closely resembles the experimental situation. Defect free BaO surfaces are difficult to prepare, and NO_x storage experiments are in most cases conducted on BaO dispersed on a high surface γ-Al_2O_3 support material, which does not show any high degree of translational order.

In the study using the slab approach, the main focus was to determine the relative stability of different NO_x configurations on a thin BaO(1 0 0) surface film. BaO(1 0 0) is the BaO surface with lowest surface energy. Ultrasoft pseudopotentials according to Vanderbilt [21] were used, and the kinetic energy cut-off for the expansion of the electronic wave functions was 300 eV together with a *k*-point spacing of 0.05 $Å^{-1}$ for the generation of *k*-points according to the Monkhorst–Pack scheme [22]. Small slab models were investigated. The BaO(1 0 0) surface were modeled using a $p2 \times 2$ supercell with two atomic layers (8 MeO units), frozen at the theoretical bulk distances together with a 9 Å vacuum width. Single and pairwise NO_2 adsorption were explored allowing the NO_2 molecules to fully relax. However, when NO_2 was adsorbed over a surface oxygen anion, also the surface oxygen was structurally relaxed.

Using the cluster approach, the vibrational properties of adsorbed NO_x species were studied. Here (for technical reasons), norm-conserving Troullier–Martins [23] pseudopotentials were employed to describe the valence–core interaction. The kinetic energy cut-off was in this case 844 eV. These calculations were performed without periodic boundary conditions. The vibrational modes were calculated via numerical derivatives. Two different isomers of one cluster size was investigated, namely the "slab" and hexagonal isomers of $(BaO)_9$. These isomers were chosen because they possess several different adsorption sites. Moreover, these isomers have previously been shown to represent relevant growth paths for $(BaO)_x$ clusters, and in the case of $(BaO)_9$ being nearly energetically degenerated [24].

In the studies reported here, the gradient corrected exchange-correlation functional proposed by Perdew et al. [25] have been used (PBE). The effect of functional on physical and chemical properties for BaO have been discussed in detail in other reports [26,27].

2.2. Experimental methods

2.2.1. Flow reactor measurements

To study the stability of adsorbed NO_2, we performed temperature programmed desorption (TPD) measurements of NO_2 adsorbed on a BaO/Al_2O_3 monolith sample [5]. The catalyst was prepared by wet deposition methods. The resulting wash-coat consisted of 20 wt.% BaO and 80 wt.% γ-Al_2O_3 [28].

The experiments were initiated by a conditioning of the sample at 600 °C in Ar. NO_x storage was thereafter studied by introducing 500 ppm NO_2 in Ar for 10 min, followed by one minute in Ar, and a temperature ramp (5 °C/s) in Ar. The desorbing NO and NO_2 were measured in situ using a chemiluminescence detector [29].

2.2.2. DRIFT measurements

In situ diffuse reflectance infrared fourier transform (DRIFT) spectroscopy is a convenient method for the characterization of adsorbed molecules on catalyst surfaces. In Ref. [6] this technique was used for the identification of NO_x species during NO_2 adsorption on a BaO powder sample. In particular, we used a BioRad FTS6000 FTIR spectrometer equipped with a continuous flow reaction chamber. The vibrational spectroscopy was complemented by mass spectrometry analysis, giving the possibility to study, for example, NO desorption during NO_2 storage. To avoid contamination of CO_2 in air, the powder BaO sample was prepared in a glove box under nitrogen atmosphere. The experiments were conducted by allowing NO_2 adsorption at different temperatures, and temperature ramps in Ar to study possible surface reactions. Experimental details can be found in [6]. The background spectrum was measured at the

temperature where NO_2 adsorption was studied. The same background spectrum was used for the temperature ramp.

3. Results and discussion

3.1. Adsorbent and adsorbate properties

3.1.1. BaO—bulk, surface and cluster

BaO is an alkaline earth metal oxide with a (at normal pressure and temperature) cubic NaCl bulk structure. It is a highly ionic material with a narrow oxygen 2p valence band [27] and large experimental band-gap, 4.8 eV [30]. Our calculation of BaO in the bulk phase gives 5.59 Å, 9.6 eV and 0.7 Mbar, for the lattice constant, cohesive energy and bulk modulus, respectively [27]. Experimentally, the corresponding values are reported to 5.50 Å, 10.0 eV and 0.8 Mbar [31–33]. Thus, the computational approach (here with ultrasoft potentials) are in good agreement with experiments.[1] The slight underestimation of the energetic properties and overestimation of the lattice parameter is a usual behavior of the PBE exchange-correlation functional [25,27,34]. The large lattice parameter leads to a low restoring Madelung potential in comparison with, for example, MgO, having a lattice parameter of 4.30 Å (using the PBE functional [27]). This implies that oxygen anions in a BaO lattice will be more easily reduced in the presence of an oxidant, e.g. NO_2, than oxygen anions in MgO. This fact will be of importance when discussing the mechanistic understanding of NO_x storage.

The (1 0 0) surface is the most stable surface of BaO with a surface energy calculated to 0.4 J/m^2. This is half of the surface energy calculated for the (1 1 0) facet [27]. When characterizing structural properties of oxide surfaces, one has to consider that the surface consists of cations and anions, which respond differently to the loss of periodicity in one dimension. Consequently, the structural distortions are divided into relaxation and rumpling. Relaxation refers to the average displacement of complete atomic layers in comparison to bulk values in the direction normal to the surface. Rumpling, on the other hand, refers to the displacement of the anion with respect to the cation. A positive rumpling refers to an outward relaxation of the anion in comparison to the cation. BaO displays the largest relaxation in the series MgO, CaO, SrO and BaO. It also displays the largest rumpling (negative). A more detailed discussion regarding surface and bulk properties can be found in Ref. [27].

BaO clusters have previously been studied theoretically in the literature [24]. For $(BaO)_9$, two relevant isomers exist. One hexagonal cluster and a cluster cut out from the BaO bulk structure ("slab"). In agreement with previous studies [24] we calculate these isomers to be energetically nearly degenerated [6]. The total energies were within 0.01 eV. It is interesting that also for the slab cluster a large negative rumpling is calculated. In fact, the structural trend calculated for surfaces of the alkaline earth oxides [27] are relevant also for clusters [24].

3.1.2. The NO_2 molecule

NO_2 has C_{2v} symmetry and an odd number of electrons implying an electronic doublet state [35]. The angle and bond length is calculated to 134.2° and 1.21 Å, respectively [6]. The experimental values are 134.3° and 1.20 Å [35]. The NO_2 molecule has an experimental electron affinity of 2.27 eV, which should be compared to the electron affinity of NO and NO_3 which have values of ∼0 and 3.91 eV, respectively [36,37]. Using the present computational method (as in Ref. [6]), the electron affinity for NO_2 is computed to 2.44 eV. The electron affinity is an important parameter in the mechanistic understanding of NO_x storage on BaO, which will be discussed further below.

Since this paper deals with the characterization of molecules using DRIFT spectroscopy, it is of interest to know vibrational wavenumbers for different N–O stretch modes for the NO_x molecules. For NO_2, 1319, 742 and 1648 cm^{-1} are calculated for the symmetric, bend and asymmetric vibrational modes, respectively [6]. The corresponding experimental values are 1325, 750 and 1612 cm^{-1} [38]. For NO, the calculated [6] and experimental [38] wavenumbers for the N–O stretch mode are 1839 and 1876 cm^{-1}, respectively. Thus, the calculated wavenumbers are in difference with the experimental data by ∼40 cm^{-1}. The error is not systematic, and therefore, not possible to correct for. Consequently, our focus is more on trends in vibrational spectra than absolute wavenumbers.

3.2. Adsorption of NO_2 on BaO

In Fig. 2a and b, we show the structural results for single and pairwise NO_2 adsorption on the BaO(1 0 0) surface. Two adsorption sites are explored, atop barium and atop oxygen, respectively. The calculated adsorption energies for NO_2 over these sites are similar, −0.8 and −0.7 eV. However, despite the similar adsorption energetics, the two adsorption configurations differ significantly in chemical interaction.

Adsorption of NO_2 over a surface oxygen site creates a formal surface NO_3^{2-} species ($O_2N–O_{surf}$). The $N–O_{surf}$ bond length is 2.39 Å, which indicates some covalent character in the chemical bond. The assignment of a NO_3^{2-} species can also be made by studying the spin density for this adsorption configuration. It is found that the electronic spin is localized over the adsorbed NO_2 and the adsorption site (O^{2-}) [5,6]. In contrast to the formation of an electronically local species, adsorption of NO_2 over a barium site creates a delocalized electron hole among the surrounding surface oxygen ions, forming an adsorbed nitrite (NO_2^-). This means that the formation of nitrites over BaO(1 0 0) is done by electron transfer from the surface oxygen ions to the adsorbed NO_2 molecules. The bond distance is in this

[1] Using the Troullier–Martins pseudopotentials as in Ref. [6], the BaO cohesive energy and lattice constant are calculated to 9.76 eV and 5.59 Å, respectively.

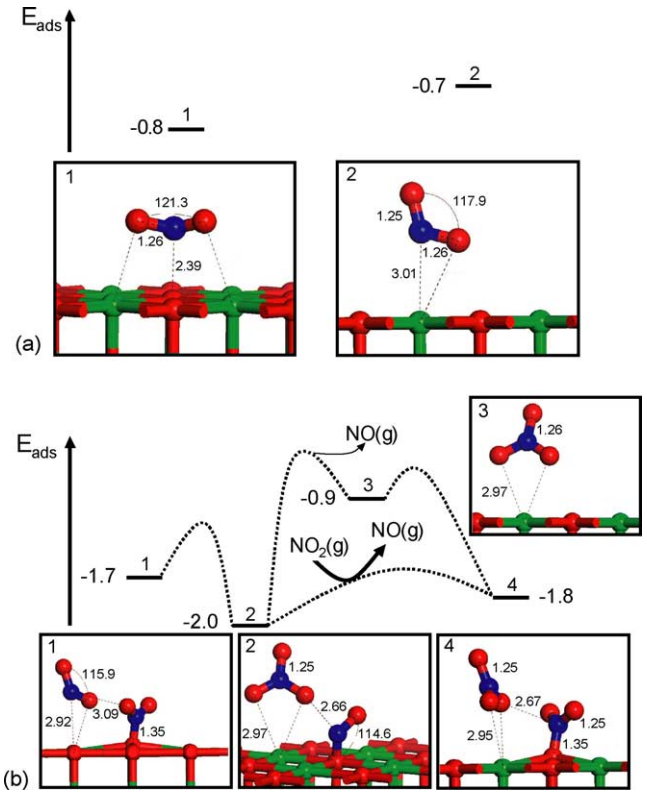

Fig. 2. Potential energy diagram for the xNO$_2$/BaO(1 0 0) system calculated using the slab representation of the BaO(1 0 0) surface. (a) Single NO_2 adsorption over a surface oxygen site and a surface barium site. Energies in eV/NO_2. (b) Pairwise NO_2 adsorption on the BaO(1 0 0) surface. Energies in eV/2NO_2. Bond lengths are in Å. Color code: green is barium, red is oxygen and blue is nitrogen.

case long, ∼3 Å, indicating an ionic interaction between the nitrite and the barium surface site. We believe that the latter configuration is important for storage of NO_2. This step also points out a clear difference between the storage of NO_x and, for example, the trapping of SO_x [39]. By creating an electron hole among the surrounding oxygen ions, the surface valence electron distribution is disturbed, i.e. there will be unoccupied O_{surf} (2p) valence states at the Fermi level in the DOS. Hence, these oxygens are activated towards further NO_2 adsorption, forming nitrate species (O_2–N–O_{surf}) in conjunction with the adsorbed nitrite over a barium site, cf. Fig. 2b. It is not clear if the formation of the O_2–N–O_{surf} species is associated with an activation barrier.

The activation of the surface oxygen ions is demonstrated by an additional energy gain calculated for the pairwise adsorption of NO_2. For the slab calculations, the additional gain is 0.3 eV/2NO_2 in comparison to single NO_2 adsorption. For the cluster calculations the additional gain is 1.4 eV/2NO_2. These values can, in some sense, be regarded as lower and upper limits for the pairwise adsorption. The slab calculations underestimate the additional gain due to the small unit cell (corresponding to a very high coverage) giving a high inter-adsorbate repulsion. Moreover, only a limited surface relaxation was allowed in these calculations. The cluster calculations, on the other hand, overestimate the pairwise effect with respect to a surface as no lateral NO_2–NO_2 repulsive interaction is present and full structural relaxation was considered. Moreover, a larger binding energy to the cluster is expected owing to the inherent instability of small clusters.

Experimental results suggest that the final storage product is surface Ba(NO_3)$_2$ [40–42]. In Fig. 2b, a reaction sequence from NO_2–BaO–NO_2 to Ba(NO_3)$_2$ is suggested. The first step is a redox reaction among the two adsorbed NO_2 molecules. One NO_2 is reduced (leaving ON–O_{surf}) whereas the other NO_2 is oxidized (resulting in NO_3). Thus, one oxygen is transferred from the O_2N–O_{surf} species to the NO_2–Ba species, forming a NO_3–BaO–NO surface complex. This configuration is 0.3 eV more stable than the initial NO_2–BaO–NO_2 surface complex [5]. A similar energy difference was calculated for the redox reaction product on the $(BaO)_9$ clusters [6]. In order to form the surface Ba(NO_3)$_2$ complex, a third NO_2 is used to oxidize the ON–O_{surf} species to form a O_2N–O_{surf} species and a NO(g). This is, however, a configuration which is less stable than the redox reaction product. The surface Ba(NO_3)$_2$ complex displays similar stability as the initial NO_2–BaO–NO_2 configuration. Furthermore, in Ref. [5], we discussed a different reaction channel, involving the formation of a surface peroxide and NO (g) from the adsorption of the second NO_2 molecule. However, it was shown that the formation of a surface peroxide is an endothermic process with respect to the formation of the NO_2–BaO–NO_2 configuration (∼1.5 eV/2NO_2). Based on this it was suggested that peroxide formation should be unstable towards surface nitrate formation.

Thus from theory, an adsorption sequence has been suggested including the formation of nitrites, cf. Fig. 2a, followed by the formation of nitrite–nitrate, nitrate–nitrite and nitrate–nitrate pairs on the surface (cf. (1), (2), (4) in Fig. 2b, respectively). The formation of a nitrate–nitrate pair is supported by flow reactor measurements, showing NO formation during NO_2 adsorption on a BaO/Al_2O_3 monolith catalyst at 300 °C (cf. Fig. 3a). As discussed above, the formation of NO during the storage of NO_2 over BaO, may also indicate the formation of surface peroxides. The storage period in Fig. 3a was followed by a temperature programmed desorption ramp, shown in Fig. 3b. In the figure, both NO and NO_2 desorption is observed, which is indicative of different adsorption configurations of NO_x species on the surface. To make connection with the presented theoretical results: We predict the stability of the adsorption configurations that may produce NO_2 to be 0.7–1.0 eV. The NO_2 is formed from nitrite desorption (cf. Fig. 2a and (1) and (4) of Fig. 2b) and/or surface nitrate decomposition, i.e. O_2–NO_{surf} → O_{surf} + NO_2 (the O_2N–O_{surf} are from (1) and (4) in Fig. 2b). The stability for the adsorption configurations that may produce NO are in the range of 0.9–1.1 eV. The NO is formed from thermal decomposition of NO_3, i.e. NO_3 → NO + O_2 (cf. NO_3 producing configurations ((2), (3) and (4)) in Fig. 2b), and/or, surface nitrite decomposition, i.e. ON–O_{surf} → O_{surf} + NO (cf. (2) in Fig. 2b). The

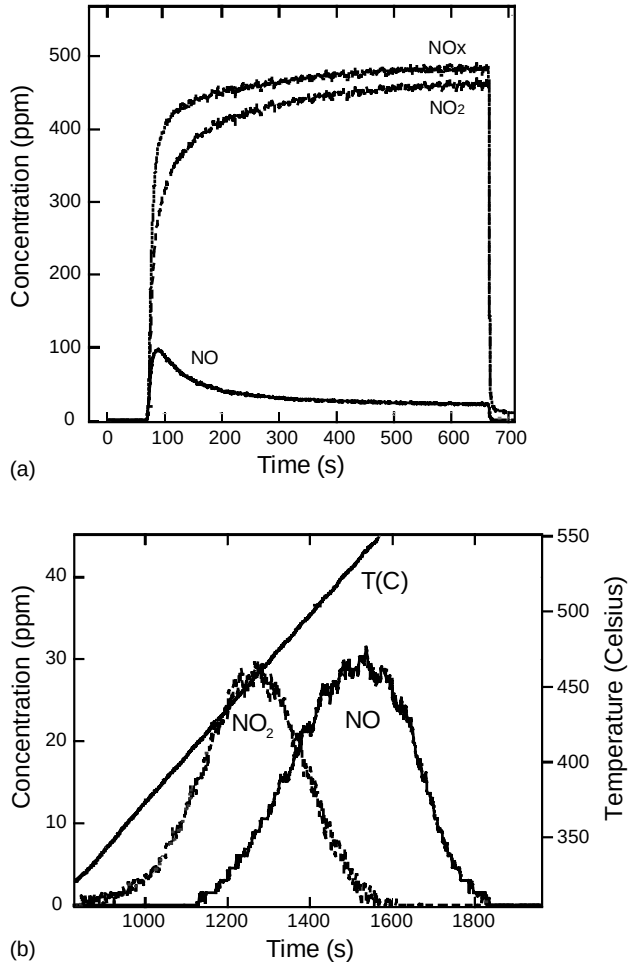

Fig. 3. (a) Storage of NO_2 over a BaO/Al_2O_3 monolith catalyst at 300 °C. (b) Temperature programmed desorption measurements of the stored NO_2 in (a).

trend in calculated relative stabilities are in agreement with the trend found in the TPD measurements, which show a NO_2 peak followed by a NO peak upon increasing the temperature. It should also be noted that some of the observed NO is likely due to NO_2 reduction after desorption, which is thermodynamically favored at these temperatures.

3.3. Characterization of NO_x species adsorbed on BaO

From the adsorption studies, we have established a mechanistic understanding of the interaction between NO_2 and BaO. The natural continuation is to find further experimental, as well as, theoretical support for this emerging picture. Therefore, characterization experiments based on in situ DRIFT spectroscopy have been employed together with theoretical vibrational analysis [6].

The first set of experiments involved DRIFT measurements of NO_2 adsorption on BaO powder at 250 °C. Spectra recorded during 10 min at this temperature are displayed in Fig. 4a. The peak structure in Fig. 4a indicates immediate (at least on the time-scale used in these experiments) surface reactions, forming adsorbed nitrites and nitrates. This observation is in agreement with the theoretical results presented above where adsorption configurations which involves surface reactions are favored. In the literature, peaks at 1500–1400 and 1200–900 cm^{-1} have been assigned to monodentate nitrites [41]. Furthermore, ionic nitrates have been assigned to bands at 1460–1400 and 1360–1300 cm^{-1} [41]. Also bulk nitrate formation is believed to occur at this temperature, with corresponding wavenumbers at 1380 cm^{-1} [43].

However, in the calculations, also a set of possible intermediate adsorbed NO_x species were investigated, see Fig. 2. In order to study the formation of such species it was necessary to slow down the storage scenario by decreasing the temperature. Experiments were therefore done by introducing NO_2 over a fresh BaO powder sample at 30 °C for 10 min followed by a temperature ramp (5 °C/s) in Ar to 450 °C. The spectra from these measurements are shown in Fig. 4b–d. Fig. 4b shows spectra from the initial NO_2 adsorption at 30 °C. At this stage, two peaks can be observed. One large at 1337 cm^{-1} and one smaller centered around 1250 cm^{-1}. Upon increasing the temperature in Ar (cf. Fig. 4c and d), an increased splitting appears in the spectra at ∼250 °C, indicating the onset of surface reactions among adsorbates.

To make connections between the experiments and the proposed theoretical scenario, we have performed vibrational analysis on $(BaO)_9$ cluster models for the above discussed storage intermediates. On this cluster, both single and pairwise NO_2 adsorption were considered. Single NO_2 adsorption were studied on both isomers of the $(BaO)_9$ cluster (see Section 3.1.1). The study revealed that the slab clusters were significantly more stable upon NO_2 adsorption (by 0.4 eV) than the hexagonal. Therefore, the pairwise NO_2 adsorption was restricted to the slab clusters. By altering the adsorption sites on the cluster, using both a center oxygen site and an edge oxygen site, the formation of a nitrite and a formal NO_3^{2-} species were possible. These are shown in Fig. 5 and denoted 5S for the nitrite formation, whereas 3S corresponds to the formation of NO_3^{2-}. For the clusters, the formation of a nitrite (5S) is 0.4 eV more stable than the formation of a NO_3^{2-} (3S). Vibrational wavenumbers were calculated for both these species, with distinctly different characteristics. The nitrite N–O asymmetric and symmetric vibrational stretching modes were calculated to 1299 and 1304 cm^{-1}, respectively, whereas the NO_3^{2-} asymmetric and symmetric N–O stretches were found at 1384 and 1210 cm^{-1}, respectively. A graphical representation of the vibrational results for the 5S and the 3S configurations are given in panel (a) of Fig. 5.

The adsorption of a single NO_2 on the $(BaO)_9$ clusters indicated that nitrite formation was possible, in agreement with the periodic super-cell slab calculations. Therefore, we use the 5S configuration, and continue to study the pairwise adsorption. Having in mind that the adsorption energy enhancement for pairwise adsorption is an electronic odd–even effect, mediated by the oxide surface, the addition of the second NO_2 molecule to the 5S cluster was made by allowing

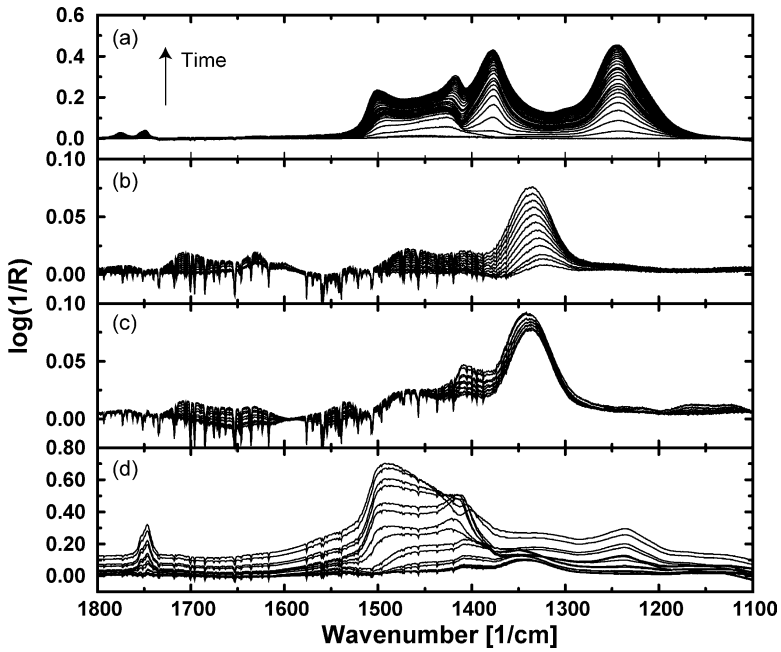

Fig. 4. Spectra for NO_2 adsorption on BaO powder. (a) At 250 °C for 20 min. Background spectra taken at 250 °C. During the first 6.5 min, spectra were taken every 30 s. Thereafter, the sampling rate was 1 min for the continuing 5 min, and 2 min for the rest of the experiment. (b) Spectra for NO_2 adsorption on BaO powder at 30 °C for 10 min. (c) and (d) spectra taken during the following temperature ramp in Ar, starting from (b). (c) refers to 30–150 °C, whereas (d) is the temperature interval 150–450 °C. Background spectra for (b)–(d) were taken at 30 °C. First three spectra for NO_2 exposure at 30 °C were taken with 30 s interval, whereas the rest of the spectra were taken every 60 s.

the second NO_2 to adsorb on a barium ion on the opposite side (cf. panel (b) of Fig. 5). This configuration reflects the nitrite–nitrate (NO_2–BaO–NO_2) pair found in the periodic slab calculations, though without lateral repulsive interactions. To further connect to the periodic slab calculations, the nitrate–nitrite pair was constructed by transferring one oxygen from the nitrate to the barium associated nitrite. Two different configurations of the latter surface complex were investigated. These are depicted in panels (c) and (d) of Fig. 5 and they differ in the location of the nitrite (ON–O_{clus}). This

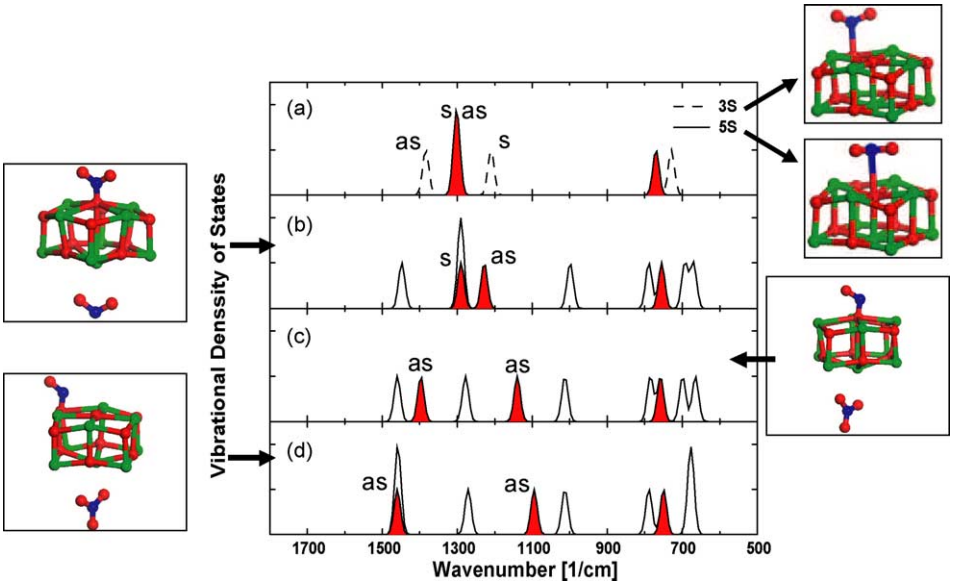

Fig. 5. Calculated vibrational density of states for the xNO_2–BaO clusters. (a) shows single NO_2 adsorption in the 3S and 5S configurations. (b) is the NO_2–BaO–NO_2 configuration. (c) and (d) display the two tested configurations of the NO_3–BaO–NO pair. Shaded area is vibrational contributions from $NO_2^{\delta-}$, $\delta \leq 1$. The figures correspond to the cluster configurations. Red is oxygen, green is barium and blue is nitrogen. AS is asymmetric stretch and S is symmetric stretch.

Table 1
Calculated asymmetric–(a)symmetric vibrational splitting for the different stable configurations of adsorbed NO_2 species depicted in Fig. 5

Configuration	Splitting (cm^{-1})
(a) 3S	174
(a) 5S	−5
(b) (Ba–NO_2)	−62
(c) (O_{5S}–NO)	−257[a]
(d) (O_{3S}–NO)	−365[a]

The character in parenthesis refers to the corresponding panel in Fig. 5.
[a] This value corresponds to the splitting between O_{clus}–N and the N–O mode.

was done in order to analyze the sensitivity of the nitrite N–O stretch vibrational modes towards different adsorption configurations.

The vibrational properties for the investigated $2NO_2$–$(BaO)_9$ compounds are summarized in the (b)–(d) panels of Fig. 5. Comparison between panels (a) and (b) reveals that there is a smaller asymmetric–symmetric band splitting calculated for the 5S nitrite configuration in comparison to the nitrite adsorbed over a barium site (shaded area in panels (a) and (b) of Fig. 5). When considering the nitrite formed upon redox reaction (shaded area in panel (c) of Fig. 5), this species does not show any symmetric vibrational mode due to the asymmetric geometry, leading to two decoupled (asymmetric) vibrational modes, ω(N–O_{clus}) and ω(N=O). The calculated splitting (ω(N–O) − ω(N=O)) for this species is even larger than for the barium associated nitrite. To test the sensitivity of the N–O stretch vibrational mode to the adsorption geometry even further, the redox-reaction product (ON–O_{surf}) was allowed to occupy an edge cluster site (bottom panel of Fig. 5). At this configuration, the splitting is larger. The calculated asymmetric–(a)symmetric vibrational splittings for the nitrite like species are summarized in Table 1.

Concerning the nitrates formed on the clusters, both monodentate and bidentate nitrates were considered (cf. Fig. 5). Comparing panels (b)–(d) of Fig. 5, we observe that all nitrates display similar vibrational characteristics, irrespective of the adsorption geometry. This can be rationalized by the high electron affinity of NO_3 and that the cluster allows large relaxation, leading to the formation of symmetric surface nitrate species, despite the inclusion of a cluster oxygen.

We would at this point like to stress that the vibrational similarity between the formed nitrate and nitrite like species upon adsorption of NO_2 on BaO will make it hard to distinguish among them in the experimental vibrational spectra. However, the nitrate should have an extra peak in comparison to the nitrite. In our experimental setup, however, this peak at $\sim$1000 cm^{-1} is for technical reasons not possible to detect.

Comparing the experimental spectra of Fig. 4b–d and the calculated spectra in Fig. 5, we find that the trend in the experiments are similar to the reaction scenario suggested by theory: At low temperatures, only nitrite formation is feasible on the surface because of the low coverage, and the possible existence of activation barriers for nitrate formation (compare Figs. 4b and 5a). However, upon temperature increase, an onset of surface reactions are found at $\sim$250 °C, cf. Fig. 4d, manifested by an increased splitting in the spectra. The splitting indicates nitrate formation on the surface, in agreement with other experimental studies [40–42]. However, as observed in the calculated spectra, the splitting is not only due to surface nitrate formation. Different configurations of $NO_2^{\delta-}$, $\delta \leq 1$, display similar vibrational splitting. This band overlap among surface nitrates and nitrites makes the assignment of specific coordination of surface species very difficult.

4. Conclusions

In this paper, we have reviewed our mechanistic understanding of NO_x storage obtained both from theoretical and experimental studies. Our present picture can be summarized as follows:

- Single NO_2 adsorption on BaO produces nitrite species by abstraction of an electron from surface oxygen ions. Thereby, a delocalized electron hole is created in the surface O(2p) states, activating oxygen toward further NO_2 adsorption.
- A second NO_2 can adsorb over an activated surface oxygen, forming a nitrate. Thereby, a nitrite–nitrate pair is formed. This step is energetically favorable in comparison to single NO_2 adsorption.
- To find a reaction pathway toward the formation of the experimentally suggested surface $Ba(NO_3)_2$ compound, a redox reaction is suggested, forming a nitrate–nitrite pair on the surface. This pair displays similar vibrational spectra as would a surface $Ba(NO_3)_2$ compound. This configuration is, moreover, the most stable configuration of two NO_2 molecules on the surface.
- To form the experimentally suggested surface $Ba(NO_3)_2$ compound, a gaseous NO_2 molecule is used to oxidize the nitrite, leaving a NO to gas phase.
- A reaction channel including the formation of a nitrite–peroxo pair on the surface was also suggested. It was found that peroxide formation is unstable toward surface nitrate formation.

To summarize and speculate how our understanding of the NO_x storage sequence can be used to improve the performance of the NO_x traps presently employed, we would like to point out the importance of the pairwise adsorption. This effect predicted first in Ref. [5] is not found for CO_x and SO_x adsorption, which are believed to be the main contaminants, hindering efficient NO_x storage. As mentioned, surface CO_x formation has been shown to be unstable towards surface nitrite formation. However, in order to find a material with an increased selectivity towards NO_x rather

than SO_x, the pairwise effect should be promoted even further.

Acknowledgements

Constructive discussions with Prof. Bengt Andersson and Prof. Bengt Kasemo are gratefully acknowledged. The calculations have been performed on IBM SP2 at PDC, Stockholm and at UNICC, Göteborg, Sweden. The Competence Centre for Catalysis is hosted by Chalmers University of Technology and financially supported by the Swedish Energy Agency and the member companies AB Volvo, SAAB Automobile Powertrain AB, Johnson Matthey CSD, Perstorp AB, Akzo Nobel Catalyst, AVL-MTC AB and the Swedish Space Corporation.

References

[1] N. Takahashi, H. Shinjoh, T. Iijima, T. Suzuki, K. Yamazaki, K. Yokota, N. Suzuki, N. Miyoshi, S. Matsumoto, T. Tanizawa, et al., Catal. Today 27 (1996) 63.
[2] W. Bögner, M. Krämer, B. Krutzcsh, S. Pischinger, D. Voigtländer, G. Wenninger, F. Wirbeleit, M. Brogan, R. Brisley, D.E. Webster, Appl. Catal. B 7 (1995) 153.
[3] F. Rodrigues, L. Juste, C. Potvin, J. Tempé, G. Blanchard, G. Djéga-Mariadassou, Catal. Lett. 72 (1–2) (2001) 59.
[4] A. Amberntsson, B. Westerberg, P. Engström, E. Fridell, M. Skoglundh, Stud. Surf. Sci. Catal. 126 (1999) 318.
[5] P. Broqvist, I. Panas, E. Fridell, H. Persson, J. Phys. Chem. B 106 (2002) 137.
[6] P. Broqvist, H. Grönbeck, E. Fridell, I. Panas, J. Phys. Chem. B 108 (2004) 3523.
[7] J.A. Rodriguez, J. Jirsak, J.Y. Kim, J.Z. Larese, A. Maiti, Chem. Phys. Lett. 330 (3–4) (2000) 475.
[8] W.F. Schneider, K.C. Hass, M. Miletic, J.L. Gland, J. Phys. Chem. B 106 (30) (2002) 7405.
[9] M. Miletic, J.L. Gland, K.C. Hass, W.F. Schneider, J. Phys. Chem. B 107 (1) (2003) 157.
[10] E.J. Karlsen, M.A. Nygren, L.G.M. Petterson, J. Phys. Chem. B 107 (2003) 7795.
[11] W.F. Schneider, J. Phys. Chem. B 108 (2004) 273.
[12] M.M. Branda, C.D. Valentin, G. Pacchioni, J. Phys. Chem. B 108 (2004) 4752.
[13] P. Hohenberg, W. Kohn, Phys. Rev. 136 (1964) 864.
[14] W. Kohn, L.J. Sham, Phys. Rev. 140 (1965) A1133.
[15] M.C. Payne, M.P. Teter, D.C. Allan, T.A. Arias, J.D. Joannopoulus, Rev. Mod. Phys. 64 (4) (1992) 1045.
[16] W. Andreoni, A. Curioni, Parallel Comput. 26 (2000) 819.
[17] D. Marx, J. Hutter, Modern Methods and Algorithms in Quantum Chemistry, Forschungzentrum Juelich NIC Series, vol. 1, 2000.
[18] CPMD v3.5 Copyright IBM Corp 1990–2001, Copyright MPI fuer Festkoerperforschung Stuttgart 1997–2001.
[19] CASTEP from Accelrys Inc.
[20] H. Grönbeck, Top. Catal. 28 (2004) 59.
[21] D. Vanderbilt, Phys. Rev. B 41 (1990) 7892.
[22] H. Monkhorst, J. Pack, Phys. Rev. B 13 (1976) 5188.
[23] N. Troullier, J.L. Martins, Phys. Rev. B 46 (1992) 1754.
[24] F. Bawa, I. Panas, Phys. Chem. Chem. Phys. 4 (2002) 103.
[25] J. Perdew, K. Burke, M. Ernzerhof, Phys. Rev. Lett. 77 (1996) 3865.
[26] H. Grönbeck, P. Broqvist, J. Chem. Phys. 119 (7) (2003) 3896.
[27] P. Broqvist, H. Grönbeck, I. Panas, Surf. Sci. 554 (2004) 262.
[28] E. Fridell, M. Skoglundh, B. Westerberg, S. Johansson, G. Smedler, J. Catal. 183 (1999) 196.
[29] M. Skoglundh, H. Johansson, L. Löwendahl, L. Jansson, L. Dahl, B. Hirschbauer, Appl. Catal. B 7 (1996) 299.
[30] V. Dimitrov, S. Sakka, J. Appl. Phys. 79 (3) (1996) 1736.
[31] Z.P. Chang, G.R. Barsch, J. Geophys. Res. 74 (1969) 3291.
[32] Z.P. Chang, E.K. Graham, J. Phys. Chem. Solids 38 (1977) 1355.
[33] M. Königstein, C.R.A. Catlow, J. Solid State Chem. 140 (1998) 103.
[34] M. Körling, J. Häglund, Phys. Rev. B 45 (1992) 13293.
[35] N.N. Greenwood, A. Earnshaw, Chemistry of the Elements, Pergammon Press, Oxford, UK, 1984.
[36] K.M. Ervin, J. Ho, W.C. Lineberger, J. Phys. Chem. 92 (1988) 5405.
[37] J.A. Davidson, F.C. Fehsenfeld, C.J. Howard, Int. J. Chem. Kinet. 56 (1977) 17.
[38] K.I. Hadjiivanov, Catal. Rev. Sci. Eng. 42 (1&2) (2000) 71.
[39] W.F. Schneider, J. Li, K.C. Hass, J. Phys. Chem. B 105 (2001) 6972.
[40] B. Westerberg, E. Fridell, J. Mol. Catal. A: Chem. 165 (1–2) (2001) 249.
[41] F. Prinetto, G. Ghiotti, I. Nova, L. Lietti, E. Tronconi, P. Forzatti, J. Phys. Chem. B 105 (2001) 12732.
[42] C. Sedlmair, K. Seshan, A. Jentys, J.A. Lercher, J. Catal. 214 (2003) 308.
[43] J.M. Coronado, J.A. Andersson, J. Mol. Catal. A: Chem. 138 (1999) 83.